8th ANKARA INTERNATIONAL AEROSPACE CONFERENCE
10-12 September 2015 - METU, Ankara TURKEY

AIAC-2015-118

EFFECT OF SPANWISE GUST ON A WING

Hülya Biler[1], Berk Zaloğlu[2] and Okşan Çetiner[3]

Istanbul Technical University
Istanbul, Turkey

ABSTRACT

In this study, a long oscillating plate is used to generate periodic continuous gusts focusing on the applications for MAVs. A flat plate that moves with a periodic function in pitch and plunge axes produces significant and distinct vortices in its wake which can simulate spanwise wind gusts. The spectral analysis of the velocity field in the wake of the airfoil is used to characterize the gust. A wing is also positioned downstream of the oscillating plate and force measurements are obtained to analyze the effect of the gust on loading.

INTRODUCTION

With the increasing significance of micro aerial vehicles (MAVs) in aviation, the effect of gust on MAV aerodynamics becomes an important consideration. Because of their size and the low Reynolds number of their flight envelop, MAVs are more susceptible to gusts [Viswanath and Tafti, 2010]. MAVs as well as insects and birds face a considerable challenge in sudden wind gust situations that test their capability to maneuver a desired flight path [Watkins et al., 2006]. The sudden change in wing loading coupled with their inherent small inertia, can immediately affect flight stability. Stability in wind gust situations becomes very important, especially when they constitute a significant percent of the airspeed of the MAV [Viswanath and Tafti, 2010].

Although numerical studies [Yang and Obayashi, 2004; Viswanath and Tafti, 2010; Jones and Yamaleev, 2012] on the effect of gust on the aerodynamics of MAV have been conducted in the past decade, experimental studies on the subject were seldom. The reason behind has been mostly the difficulty of simulating a controllable uniform gust. A typical wind tunnel intends to reduce the perturbations within the flow which is far away from the conditions which MAVs operate. Instead a wind tunnel should simulate the atmospheric conditions that involves gust [Roadman and Mohseni, 2009].

Around 1915 the NACA started its survey on atmospheric turbulence and gusts models [Murrow et al., 1989]. First analytic models are based on discrete gusts which involve a one-time finite change in velocity [Roadman and Mohseni, 2009]. Gusts are usually presented as a sudden added component in the parallel or perpendicular direction to the freestream velocity. However, it is obvious that this model is not appropriate for some applications. MAVs usually have to operate in continuous wind gusts than discrete ones. Generalized harmonic analysis is used to specify superimposed sinusoidal gusts of various frequencies and phases in a spectrum of gusts approximating that found in nature [Roadman and Mohseni, 2009]. Today, both discrete and spectral gust analysis are employed in aircraft design [Fuller, 1997].

In NACA Gust Tunnel discrete gusts have been generated using an external jet [Donely, 1939] and in others using oscillating slats which are the two best methods found for producing discrete gusts [Roadman and Mohseni, 2009]. On the other hand, continuous gusts are mostly generated by using

[1] Undergraduate Student, Department of Aeronautical Engineering, Email: hulyabiler@gmail.com
[2] Researcher, Trisonic Lab., Faculty of Aeronautics and Astronautics, Email: berk_zaloglu@yahoo.com
[3] Professor, Department of Astronautical Engineering, Email: cetiner@itu.edu.tr

passive grids [Compte-Bellot and Corrsin, 1966; Compte-Bellot and Corrsin, 1971]. However for a given flow velocity, these passive grids are unable to adjust turbulence levels where the length scale of turbulence is related to the mesh spacing. Whereas active grids are capable of adjusting turbulence levels for a given flow speed and generating larger length scales than passive grids [Roadman and Mohseni, 2009].

In this study, another approach suggested by [Biler, et al., 2014] is used for active generation of periodic continuous gusts focusing on the applications for MAVs. An airfoil that moves with a periodic function in pitch and plunge axes produces significant and distinct vortices in its wake which can simulate spanwise wind gusts. The spectral analysis of the velocity field in the wake of the airfoil can be used to characterize the gust. A wing is also positioned downstream of the oscillating plate and force measurements are obtained to analyze the effect of the gust on loading.

METHOD

The experimental study is conducted in the closed-circuit, large scale, free-surface water channel located in the Trisonic Laboratories at the Department of Aeronautics and Astronautics Engineering of Istanbul Technical University. The cross-sectional dimensions of the main test section are 1010mm x 790mm. A flat plate is used to generate spanwise gust. The flat plate is made of Plexiglas with a span of 400mm and chord of 100mm. Its thickness is 5mm; both of its edges are sharpened approximately with a 30 degrees slope. This flat plate is mounted in the water channel at its half chord in a vertical cantilevered arrangement. The connection rod connects the flat plate to a servo motor which provides the pitching motion and this servo is also connected to a linear table which provides the plunging motion. The wing behind the oscillating plate is absent during the gust characterization experiments.

A Digital Particle Image Velocimetry (DPIV) system is used to acquire the vector fields in the wake of the oscillating flat plate. The flow is illuminated by a dual cavity Nd:Yag laser (max. 120 mJ/pulse) and the water is seeded with silver coated glass spheres of 10μm diameter. Two 10-bit cameras with 1600×1200 pixels resolution are positioned under the water channel. The two double frame images from the two cameras are stitched before the interrogation using an in-house code and the resulting PIV images are interrogated using a double frame, cross-correlation technique with a window size of 64×64 pixels and 50% overlapping in each direction. The final grid resolution of velocity vectors is 3.2mm × 3.2mm in the plane of the flow and the resulting measurement plane is represented with 3264 velocity vectors. The experimental arrangement is shown in Figure 1.

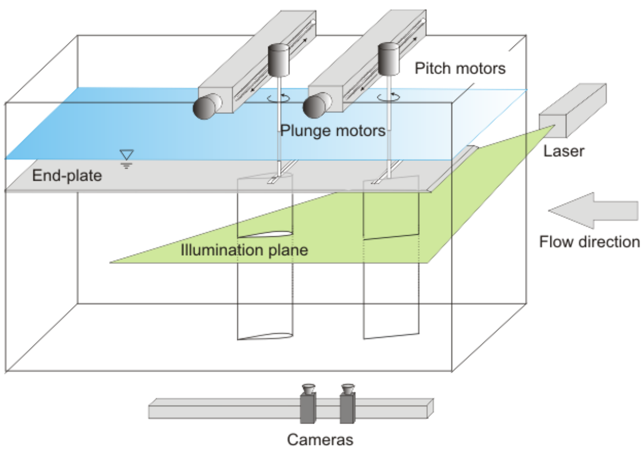

Figure 1: *Experimental Setup*

The flat plate model undergoes pitching and plunging motion that can be described with the following equations:

$$\alpha(t) = \alpha_0 + \alpha_{amp}\cos(2\pi f\, t)$$

$$h(t) = h_{amp}\sin(2\pi f\, t)$$

where *h(t)* is the linear plunge motion, perpendicular to the freestream velocity, *α(t)* is the angular pitch motion. h_{amp} is the plunge amplitude, α_{amp} is the pitch amplitude and α_0 is the initial angle of attack. *f* is the common frequency for both for plunge and pitch motion. In some cases, cosine and sine wave signals are replaced with square and triangle wave signals respectively as shown in Figure 2. These cases are studied to investigate the effect of a more rapid change at the apices of the motion to the gust characteristics. The water channel velocity is 0.1m/s which corresponds to a Reynolds number of 10000. The amplitude of the plunge motion is calculated in accordance with the frequency and the pitch amplitude, so that the feathering conditions are met in the linear displacement patterns (square and triangle wave signals). The values are kept the same for the sinusoidal patterns as well (cosine and sine wave signals). In total 20 cases are investigated with different motion parameters (Table 1).

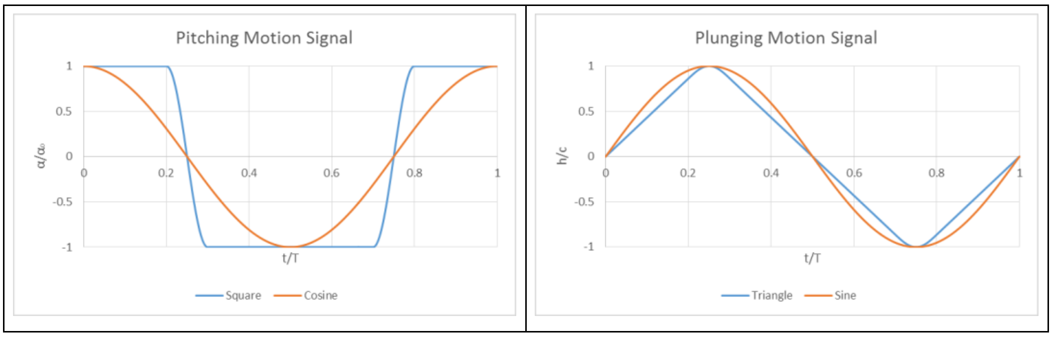

Figure 2: *Pitching and plunging motion signals*

Case	Velocity [m/s]	Frequency [hz]	Alpha Offset [deg]	Alpha Amp [deg]	h Amp (mm)	Pitch	Plunge
1	0.10	0.25	0	45	X	Square	X
2	0.10	0.5	0	45	50.2	Cosine	Sine
3	0.10	0.25	0	45	100.4	Square	Triangle
4	0.10	0.25	0	45	100.4	Cosine	Sine
5	0.10	0.25	0	30	X	Square	X
6	0.10	0.5	0	30	28.98	Cosine	Sine
7	0.10	0.25	0	30	57.96	Square	Triangle
8	0.10	0.25	0	30	57.96	Cosine	Sine
9	0.10	0.25	90	-45	100.4	Square	Triangle
10	0.10	0.25	90	-45	100.4	Cosine	Sine
11	0.10	0.25	90	-60	57.96	Square	Triangle
12	0.10	0.25	90	-60	57.96	Cosine	Sine
13	0.10	0.25	180	-135	100.4	Square	Triangle
14	0.10	0.25	180	-135	100.4	Cosine	Sine
15	0.10	0.25	180	-150	57.96	Square	Triangle
16	0.10	0.25	180	-150	57.96	Cosine	Sine
17	0.10	0.25	-180	225	100.4	Square	Triangle
18	0.10	0.25	-180	225	100.4	Cosine	Sine
19	0.10	0.25	-180	210	57.96	Square	Triangle
20	0.10	0.25	-180	210	57.96	Square	Triangle

Table 1: *Motion parameters for the gust generating flat-plate*

The DPIV system is synchronized with the motion system, so that the image acquisition starts at the beginning of the third period of the gust generator motion. For each case, 400 image couples are collected with a sampling rate of 4Hz. The time between the image couples is 1000μs.

In the second part of the study, the wing with a NACA0012 profile is mounted at its quarter chord to a pitching servo motor downstream of the symmetry axis of the plunge motion of the oscillating flat plate, the distance between the connection rods are 200mm. The chord length and the span of the wing are 100mm and 300mm respectively. The distance between the trailing edge of the oscillating plate and the leading edge of the wing is 125mm at zero angle of attack. There is a six component force-moment sensor located at the connection rod between the wing and the servo motor. Force data is taken for 30 periods starting from the 5^{th} period of motion of the gust generator with a sampling rate of 10000Hz. Measurements are acquired at static angle of attacks ranging from 0° to 45°.

RESULTS

From the obtained DPIV velocity field data, 8 points are chosen for probing the horizontal and vertical velocity components (Figure 3). The frequency spectrum of each signal is then calculated. According to the dominant frequencies of the velocity fluctuations at these points, the auto-spectral density plots of the whole velocity field are derived. These plots show the distribution of the fluctuation's magnitude for a selected frequency. Furthermore cross-spectral analysis for these frequencies are carried out to demonstrate the change of phase angle of a fluctuation throughout the velocity field. The reference point for the cross-spectra plots are chosen at the symmetry axis of plunge just behind the trailing edge of the gust generating flat plate at x=10mm, y=60mm. The cross-spectra analysis of the vertical component of the velocity is calculated according to the horizontal component, whereas the horizontal component is calculated according to itself.

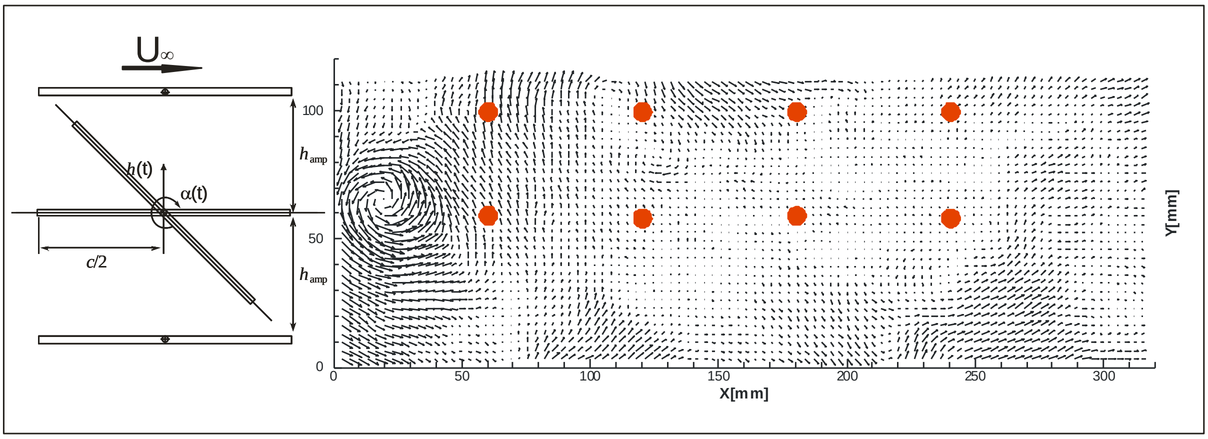

Figure 3: *Gust generator kinematics and the 8 velocity probe points*

By investing the auto-spectral density and cross-spectra plots, four cases with a uniform distribution of fluctuation frequencies and with a vertically parallel phase angle variation are selected (Table 2). The position of the wing in the flow field is also taken into consideration where the leading edge of the wing will be located at x=125mm, y=60mm for zero angle of attack in the next part of the study. The selected cases have much weaker horizontal fluctuations in the area of interest comparing to the vertical fluctuations. Thus, the cases can simulate a vertical gust, rather than a horizontal one. Gust type 1 is virtually similar with type 2 with the exception of having a frequency of 0.5Hz. All the other cases have a frequency of 0.25Hz. Gust type 3 and 4 have different motion parameters, however their auto-spectral density and cross-spectra plots have similar characteristics. In gust type 3, the flat plate makes a half backwards turn and in gust type 4, it makes a full backwards turn.

Gust Type	Case No	Velocity [m/s]	Frequency [hz]	Alpha Offset [deg]	Alpha Amp [deg]	h Amp (mm)	Pitch	Plunge
1	2	0.10	0.5	0	45	50.2	Cosine	Sine
2	4	0.10	0.25	0	45	100.4	Cosine	Sine
3	12	0.10	0.25	90	-60	57.96	Cosine	Sine
4	14	0.10	0.25	180	-135	100.4	Cosine	Sine

Table 2: *Selected gust types*

The following figures (Figure 4 and 5) exemplify one of the selected cases' results on auto-spectral density plots. Horizontal velocity fluctuations at the interested region are fairly weak, however strong and persistent vertical fluctuations are present. The dominant frequency of the vertical fluctuations is 0.5Hz and its magnitude is doubled compared to that of the horizontal fluctuations.

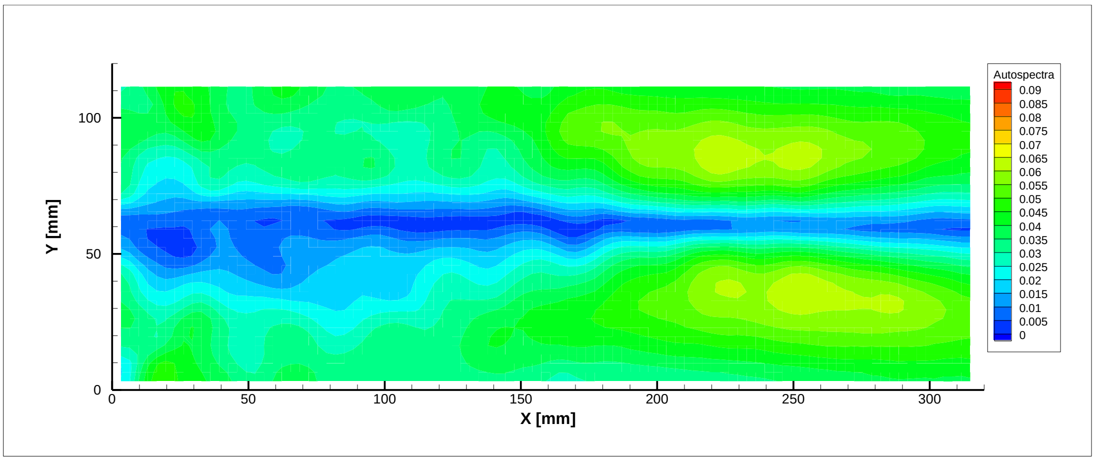

Figure 4: *Gust 1, auto-spectral density plot of horizontal velocity component*

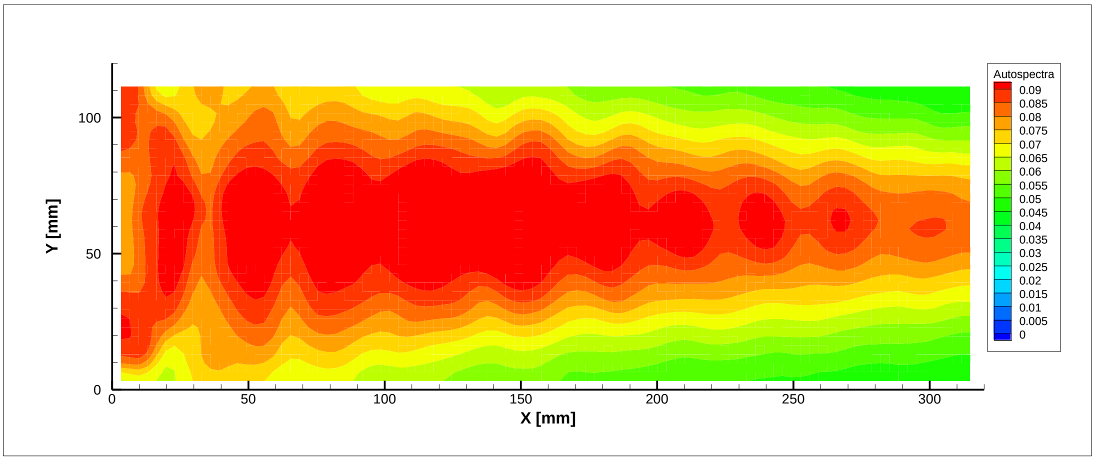

Figure 5: *Gust 1, auto-spectral density plot of vertical velocity component*

Figures 6 and 7 represent the cross-spectra plots for the same case. There is a 180 degrees phase angle between the upper and lower part of the flow field for the horizontal velocity component. For the vertical velocity component, the phase angle changes in parallel lines normal to the freestream throughout the flow field.

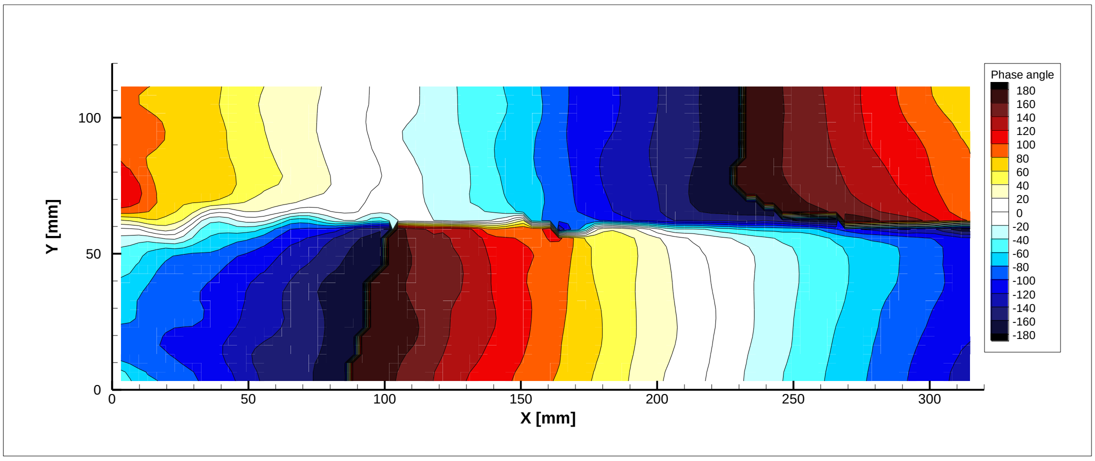

Figure 6: *Gust 1, cross-spectra plot of horizontal velocity component*

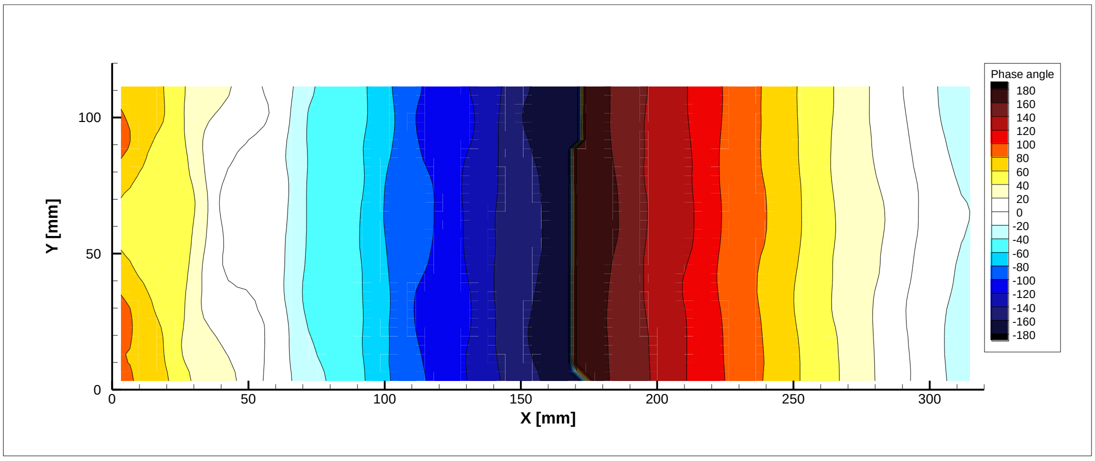

Figure 7: *Gust1, cross-spectra plot of vertical velocity component*

In Table 4, the auto-spectral density and cross-spectra plots of all four gust types are presented. However, only the vertical velocity component is essential for the evaluation of the results with the force measurements.

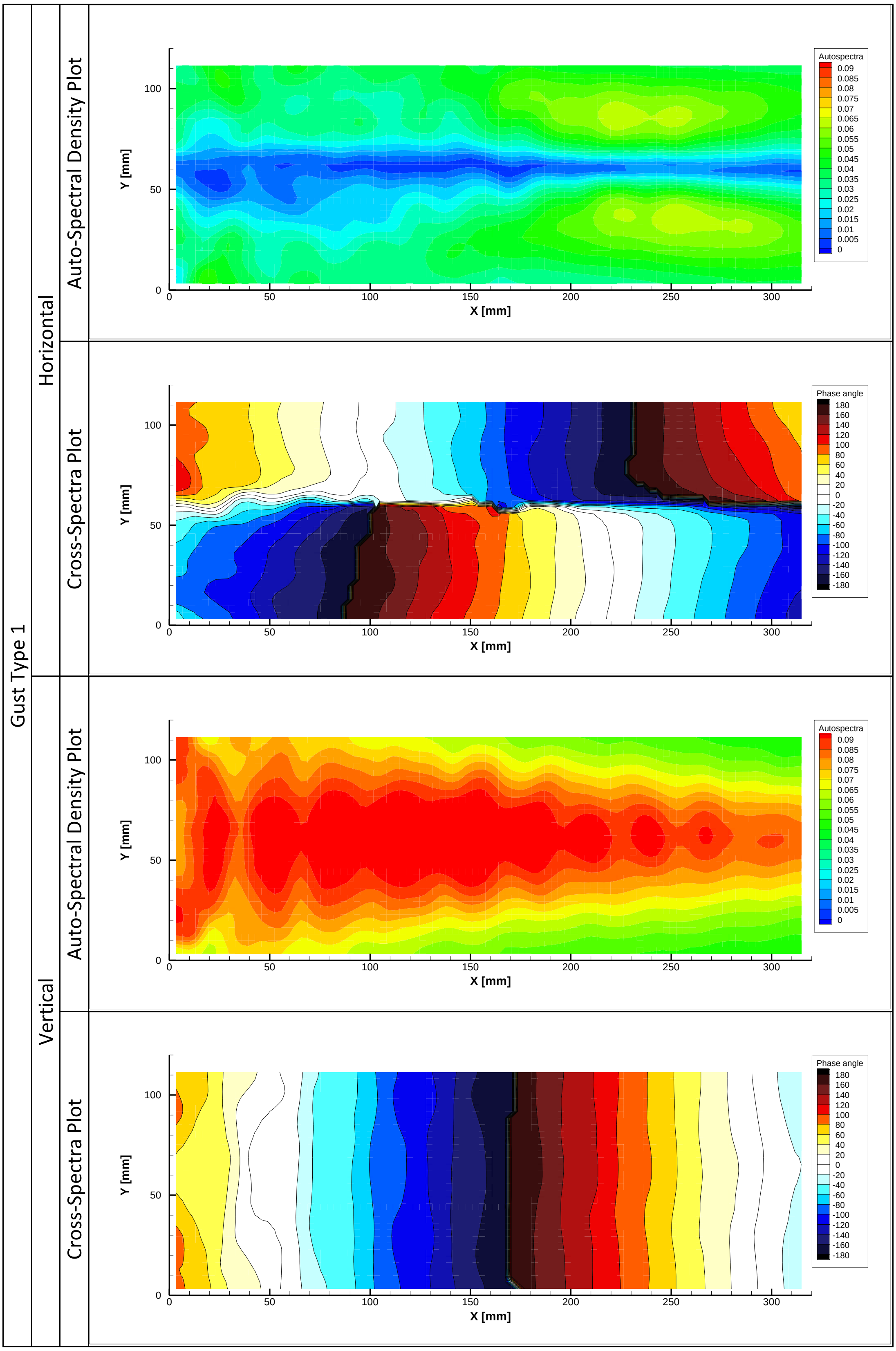
Gust Type 1
Horizontal
Vertical
Auto-Spectral Density Plot
Cross-Spectra Plot
Autospectra
0.09
0.085
0.08
0.075
0.07
0.065
0.06
0.055
0.05
0.045
0.04
0.035
0.03
0.025
0.02
0.015
0.01
0.005
0
Phase angle
180
160
140
120
100
80
60
40
20
0
-20
-40
-60
-80
-100
-120
-140
-160
-180
Y [mm]
X [mm]
0
50
100
150
200
250
300

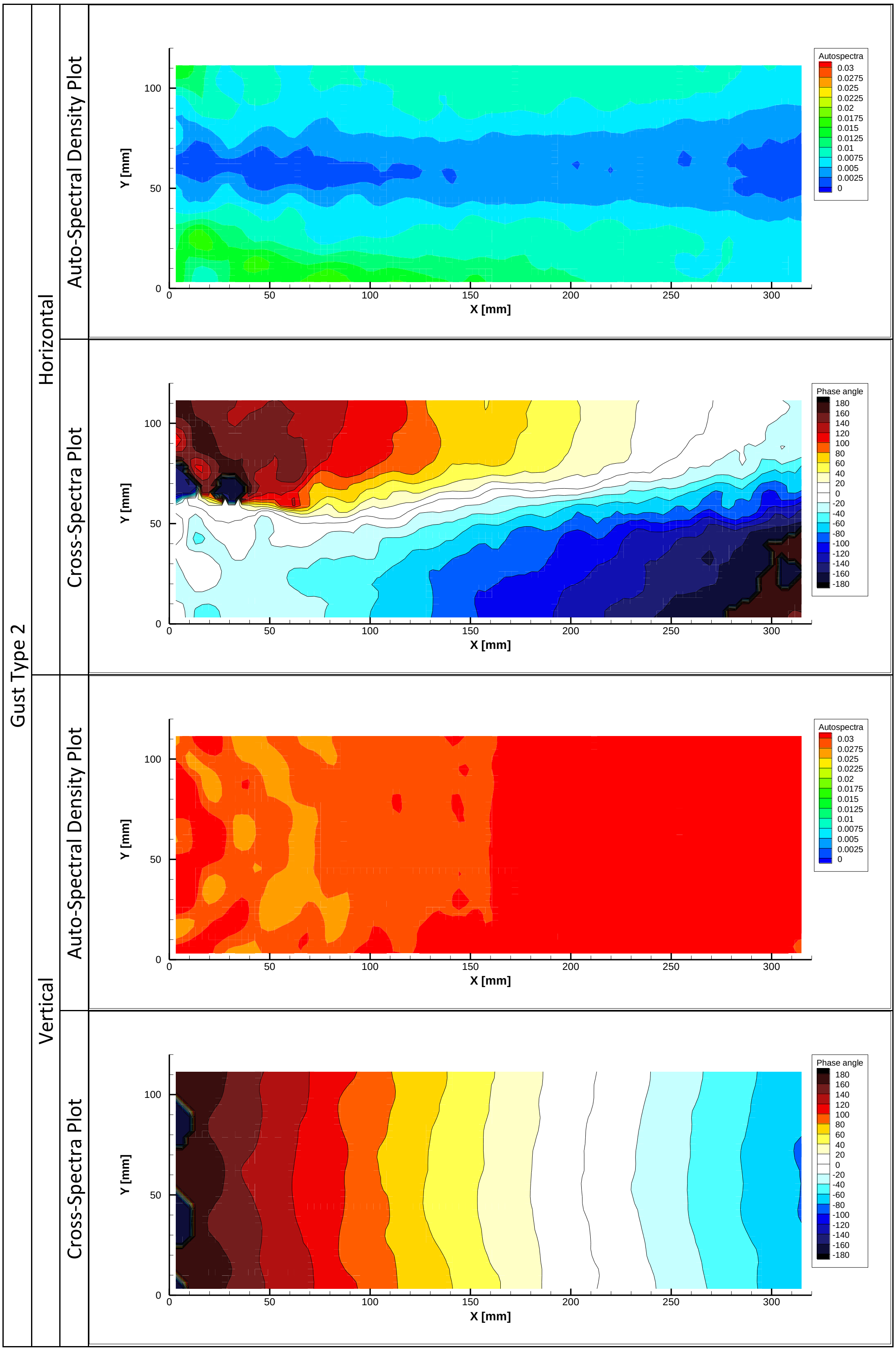

Gust Type 2
Horizontal
Vertical
Auto-Spectral Density Plot
Cross-Spectra Plot
Auto-Spectral Density Plot
Cross-Spectra Plot
Autospectra
0.03
0.0275
0.025
0.0225
0.02
0.0175
0.015
0.0125
0.01
0.0075
0.005
0.0025
0
Phase angle
180
160
140
120
100
80
60
40
20
0
-20
-40
-60
-80
-100
-120
-140
-160
-180
Y [mm]
X [mm]

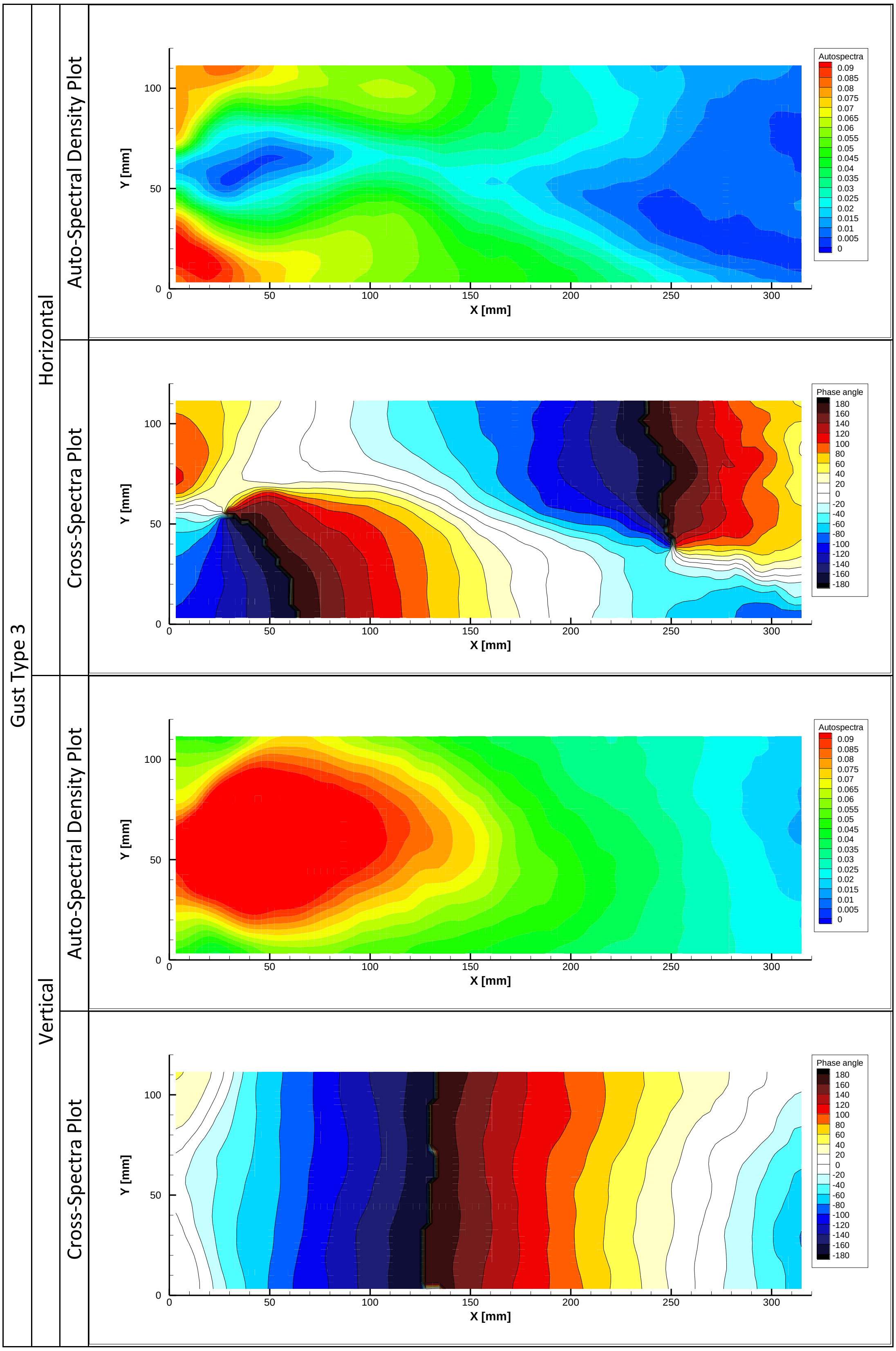
Gust Type 3
Horizontal
Vertical
Auto-Spectral Density Plot
Cross-Spectra Plot
Auto-Spectral Density Plot
Cross-Spectra Plot
Autospectra
0.09
0.085
0.08
0.075
0.07
0.065
0.06
0.055
0.05
0.045
0.04
0.035
0.03
0.025
0.02
0.015
0.01
0.005
0
Phase angle
180
160
140
120
100
80
60
40
20
0
-20
-40
-60
-80
-100
-120
-140
-160
-180
Y [mm]
X [mm]

Gust Type 4			
	Horizontal	Auto-Spectral Density Plot	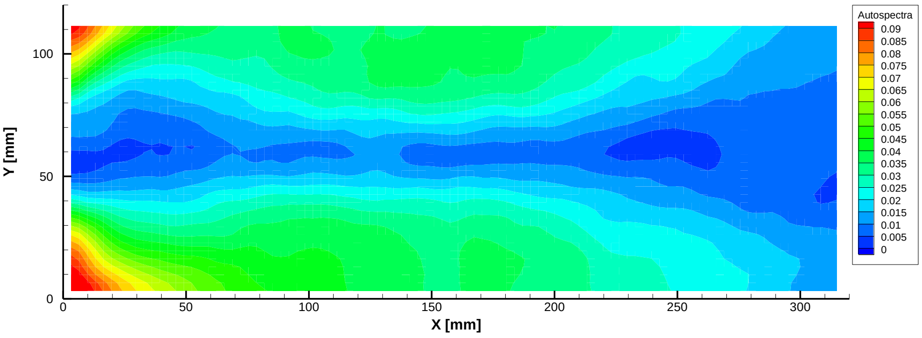
		Cross-Spectra Plot	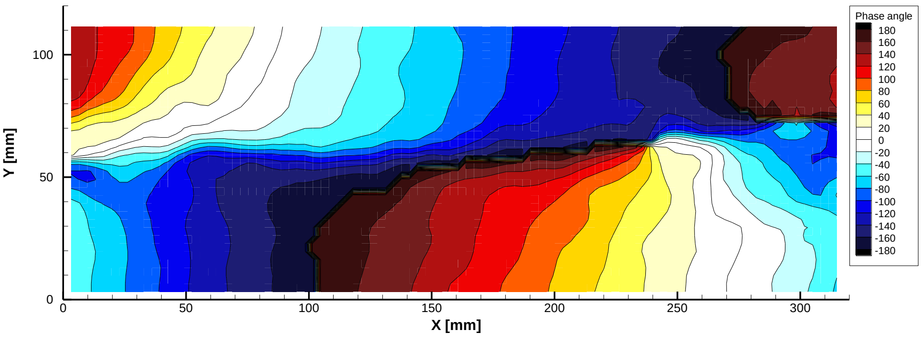
	Vertical	Auto-Spectral Density Plot	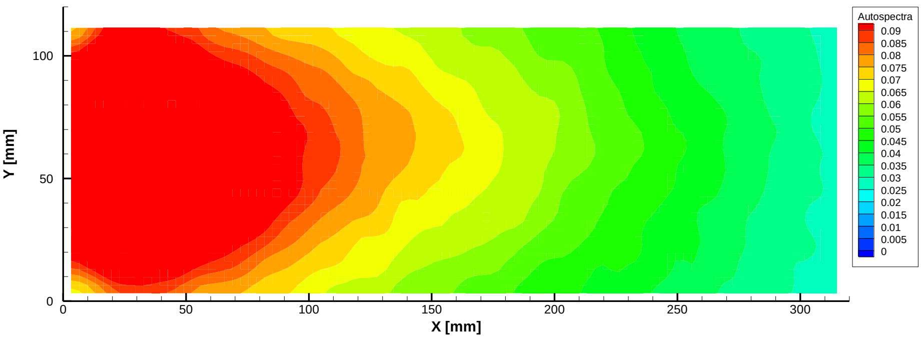
		Cross-Spectra Plot	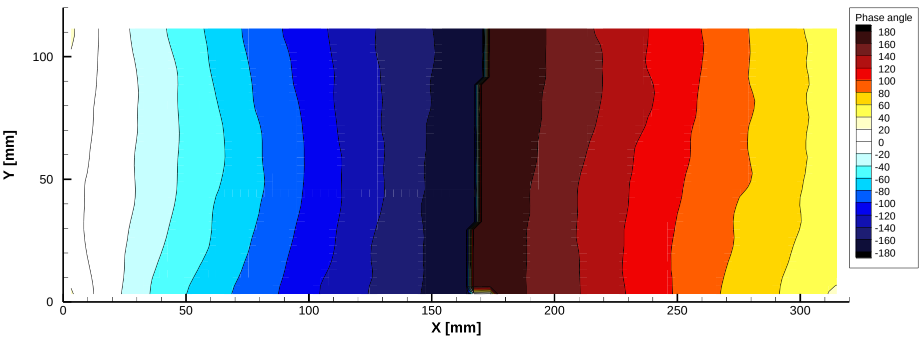

Table 4: *Auto-spectral density and cross-spectra plots of the selected cases*

The comparison of the time histories of lift acting on the airfoil at different angles of attack, between gust type 1 and 2 correlates with the vertical auto-spectral and cross-spectral plots (Figures 8 and 9). Under gust type 1, the maximum value of lift acting on the airfoil at an angle of attack of 0° is higher, more than twice the maximum value obtained under gust type 2. This relation is analogous with the auto-spectral density plot values of these two gust types. The phase angle difference between the two gusts in vertical cross-spectra plots is approximately 180 degrees at the location where the airfoil is mounted. The same phase angle difference is present for the time histories of lift acting on the airfoil. Interestingly gust type 2 has a flatter apex region than the rest of the gust types which is probably due to its wider bands of phase angle in the cross spectra plot of vertical velocity component.

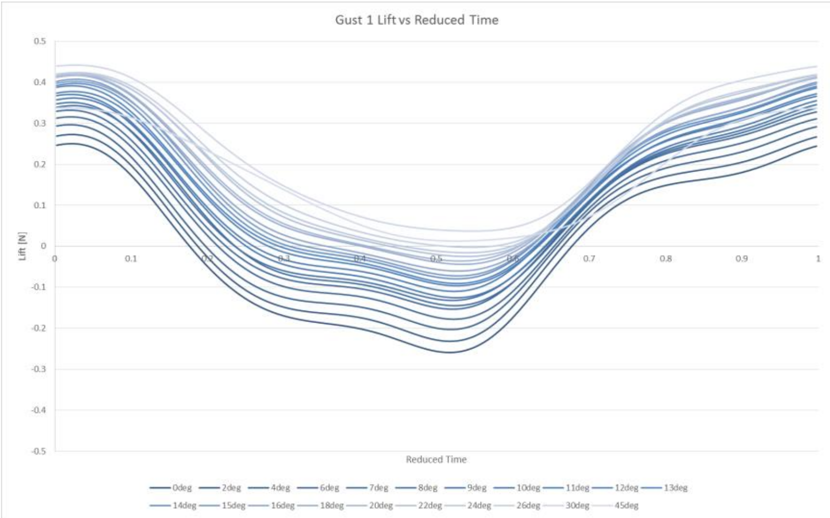

Figure 8: *Gust1, time histories of lift acting on the airfoil at different angles of attack*

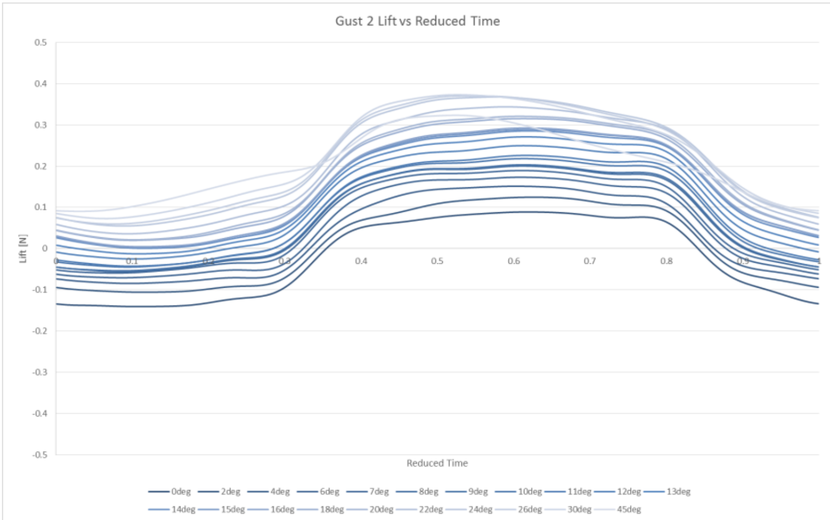

Figure 9: *Gust2, time histories of lift acting on the airfoil at different angles of attack*

The lift amplitude acting on the airfoil under gust type 4 is higher than that under gust type 3 (Figures 10 and 11). Probably, this is a result of the larger dominant area around the location where the airfoil stands in the auto-spectral density plots. The phase angle difference for the vertical velocity component between gust types 3 and 4 around x=125mm (approximately the leading edge of the wing) is around 20° which corresponds approximately to 0.05 in reduced time. The same time difference is also observed in force measurements where the maximum values of lift acting on the airfoil under gust types 3 and 4 occur around the reduced time of 0.6 and 0.55 respectively when the airfoil is at an angle of attack of 0°. The change in the lift variation with the angle of attack of the airfoil is much smaller under gust types 3 and 4 compared to the cases under gust types 1 and 2 where the lines are wider apart and therefore, under these gust types, the airfoil experiences higher lift when it is at high angles of attack.

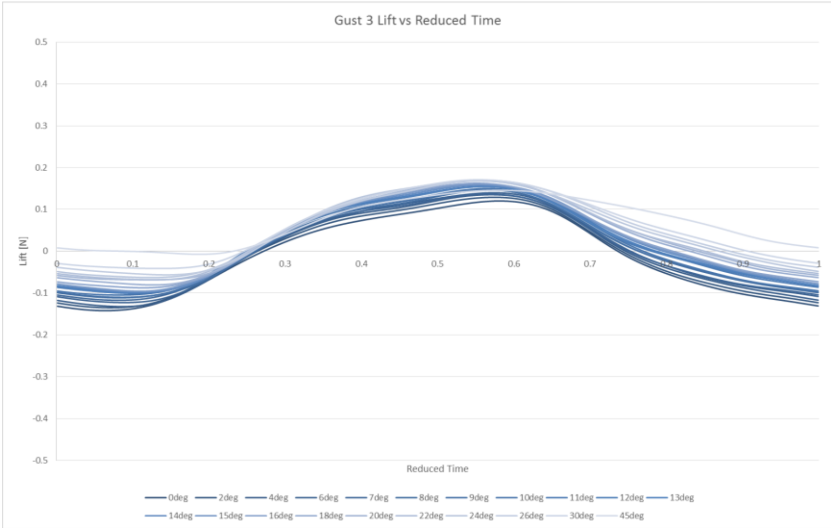

Figure 10: *Gust3, time histories of lift acting on the airfoil at different angles of attack*

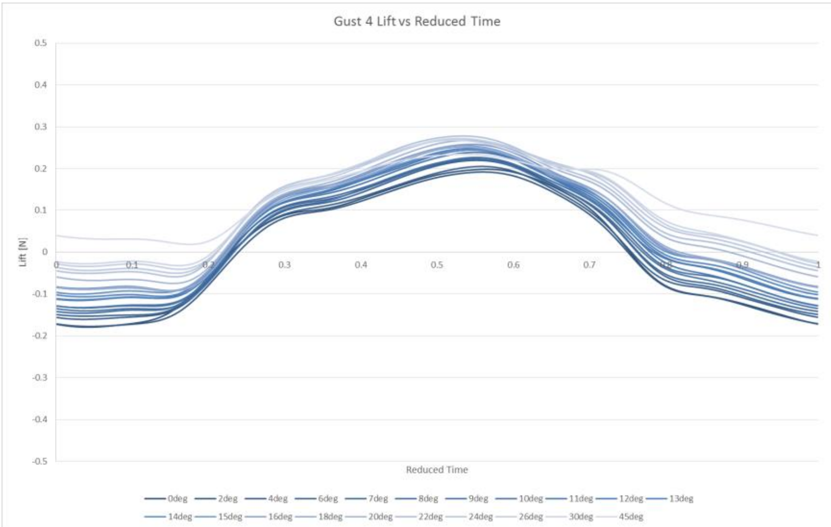

Figure 11: *Gust4, time histories of lift acting on the airfoil at different angles of attack*

The time averaged lift and drag coefficients are also calculated (Figures 12 and 13). Instead of the freestream velocity, the average value of the horizontal velocity component is used for non-dimensionalization, since the movement of the flat plate may change the average freestream velocity. Under gust types 1 and 2, the average horizontal velocity components are higher than the actual freestream value, however under gust type 3, the horizontal component of the velocity is considerably decreased. The higher lift and drag coefficients obtained when the airfoil is under gust type 3 is most probably related to the low value of the average horizontal velocity component.

For the no gust cases, the lift continue increasing till very high angles of attack without exhibiting a sudden drop for stall. Although this may seem questionable, considering that the experiments are conducted at low Reynolds numbers (Re=10000), it is correct and validated with other experimental studies [Lind et al., 2015], also conducted with a NACA0012 airfoil at low Reynolds numbers.

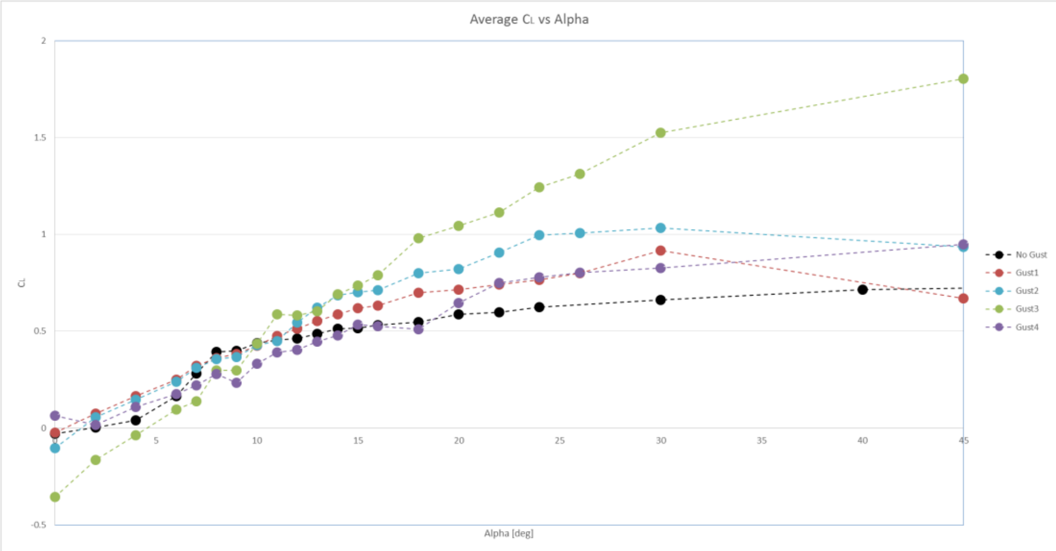

Figure 12: *Time averaged lift coefficient versus angle of attack*

The airfoil under all gust types experiences similar lift and drag coefficients when it is at low angle of attack values. However, with the increasing angle of attack values, the coefficients exhibit a considerable change. Under all four gust types, the average lift coefficient acting on the airfoil increases at high angle of attack values (Figure 12). However, this fact should not be considered as favorable, since the lift fluctuations are also considerably large in all cases.

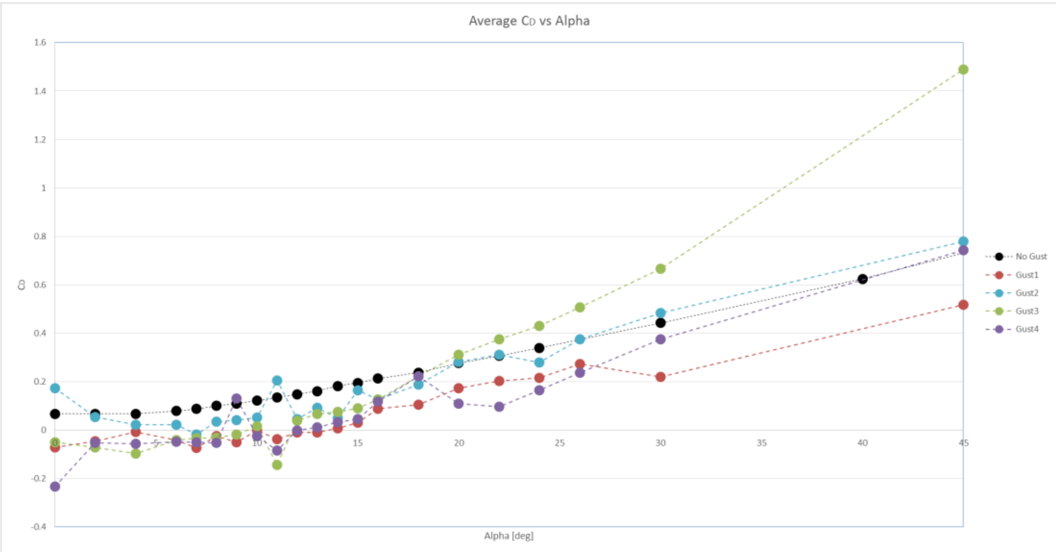

Figure 13: *Time averaged drag coefficient versus angle of attack*

CONCLUSION

A long oscillating plate is used to generate periodic continuous gusts focusing on the applications for MAVs. A flat plate that moves with a periodic function in pitch and plunge axes produces significant and distinct vortices in its wake which can simulate spanwise wind gusts. The spectral analysis of the velocity field in the wake of the airfoil is used to characterize the gust. A wing having a NACA0012 airfoil is then positioned downstream of the oscillating plate and force measurements are obtained to analyze the effect of the gust on loading. The changes in lift variation during a motion cycle of the gust generator are correlated with the gust characteristics. Although, the average lift coefficient obtained under all gust types for high angle of attack values are higher than that obtained without gust, the average drag coefficient (Figure 13) is also increasing for high angle of attack values and the time dependent lift fluctuates with large amplitudes. Therefore, time average of coefficients would be misleading in terms of the performance under gust.

References

Biler H., Zaloğlu B., and Çetiner O. (2014) *Çırpan kanatlı mikro hava araçlarının performans değerlendirmesine yönelik kontrollü sağanak oluşturulması*, V. Ulusal Havacılık ve Uzay Konferansı, Kayseri, September 2014

Compte-Bellot, G., and Corrsin, S. (1966) *The Use of a Contraction to Improve the Isotropy of Grid-Generated Turbulence,* J. Fluid Mech., Vol. 25, Issue 4, p: 657-682, August 1966

Compte-Bellot, G., and Corrsin, S. (1971) *Simple Eularian Time Correlation of Full- and Narrow-Band Velocity Signals in Grid Generated 'Isotropic' Turbulence,* J. Fluid Mech., Vol. 48, Issue 2, p: 273-337, July 1971

Donely, P. (1939) *An Experimental Investigation of the Normal Acceleration of an Airplane Model in a Gust,* NACA Technical Note, No. 706, May 1939

Fuller, J. R. (1997) *Evolution and Future Development of Airplane Gust Loads Design Requirements,* SAE Technical Paper, No. 975577, October 1997

Jones, M., and Yamaleev, N. K. (2012) *The effect of a Gust on The Flapping Wing Performance,* AIAA Paper, No. 2012-1080, 50th AIAA Aerospace Sciences Meeting including the New Horizons Forum and Aerospace Exposition, Nashville, Tennessee, January 2012

Lind, A. H., Smith, L. R., Milluzzo, J. I., Jones, A. R. (2015) Reynolds Number Effects on Airfoils in Reverse Flow, No. 2015-1973, 53rd AIAA Aerospace Sciences Meeting, Kissimmee, Florida, January 2015

Murrow, H. N., Pratt, K. G., and Houbolt, J. C. (1989) *NACA/NASA Research Related To Evolution of U.S. Gust Design Criteria,* AIAA Paper, No. 89-1373, 30th SDM Conference, Mobile, Alabama, April 1989

Roadman, J. M., and Mohseni, K. (2009) *Gust Characterization and Generation for Wind Tunnel Testing of Micro Aerial Vehicles,* AIAA Paper, No. 2009-1290, 47th AIAA Aerospace Sciences Meeting Including The New Horizons Forum and Aerospace Exposition, Orlando, Florida, January 2009

Viswanath, K., and Tafti, D. K. (2010) *Effect of Frontal Gusts on Forward Flapping Flight,* AIAA journal, Vol. 48, No. 9, p: 2049-2062, September 2010

Watkins, S., Milbank, J., Loxton, B. J., and Melbourne, W. H. (2006) *Atmospheric Winds and Their Implications for Microair Vehicles,* AIAA journal, Vol. 44, No. 11, p: 2591-2600, November 2006

Yang, G., and Obayashi, S. (2004) *Numerical Analyses of Discrete Gust Response for an Aircraft,* Journal of Aircraft, Vol. 41, No. 6, p: 1353-1359, Nov-Dec 2004